Atomic displacements and atomic motion induced by electronic excitation in heavy-ion-irradiated amorphous metallic alloys

1993 J. Phys.: Condens. Matter 5 995

(http://iopscience.iop.org/0953-8984/5/8/004)

J. Phys.: Condens. Matter 5 (1993) 995–1018. Printed in the UK

Atomic displacements and atomic motion induced by electronic excitation in heavy-ion-irradiated amorphous metallic alloys

A Audouard†, E Balanzat‡, J C Jousset‡, D Lesueur§ and L Thomé¶

† Laboratoire de Physique des Solides et Service National des Champs Magnétiques Pulsés, INSA, Complexe Scientifique de Rangueil 31 077 Toulouse, France
‡ CIRIL, Rue Claude Bloch, BP 5133, 14 040 Caen Cédex, France
§ Laboratoire des Solides Irradiés, CEA, Ecole Polytechnique, 91 128 Palaiseau Cédex, France
¶ Centre de Spectrométrie Nucléaire et de Spectrométrie de Masse, IN2P3-CNRS, Bâtiment 108, 91 405 Orsay, France

Received 29 September 1992

Abstract. In amorphous metallic alloys irradiated with swift heavy ions, electronic excitation induces atomic displacements at the beginning of the irradiation and anisotropic growth above an incubation fluence. We provide here an extensive review of our data on amorphous $Fe_{85}B_{15}$ (including work that is already published), as well as a general description of the topic. Samples were irradiated at various temperatures (20 K, 90 K, 223 K) with a large variety of high-energy (GeV) heavy ions (Ar to U). The atomic rearrangements occurring during irradiation were studied by *in situ* electrical resistance experiments. The influence of the irradiation geometry as well as of a uniaxial stress applied to the sample was investigated. The whole set of data is accounted for with a two-hit phenomenological model allowing one to extract physical parameters. A description of the ion–target interaction on the basis of the Coulomb explosion mechanism is also provided.

1. Introduction

An energetic ion which penetrates into a solid slows down via two nearly independent processes: (i) electronic excitation and ionization (electronic energy loss, $(dE/dx)_e$), dominant at high energy; and (ii) elastic collisions with the nuclei of the target atoms (elastic energy loss, $(dE/dx)_n$), dominant at low energy. Up until the 1980s most of the radiation damage studies in metals were devoted to the effects of elastic energy loss, relevant in the case of neutron or low-energy ion irradiation, since a huge technological effort was made in the framework of the evolving nuclear industry. The numerous experimental results were interpreted on the basis of accurate models (for a review, see [1]). On the contrary, in those years the study of the effects of high electronic energy loss was mainly restricted to insulators and organic materials. Two models have been proposed to account for the results obtained. The first one, by Seitz and Koehler in 1956 [2], assumes that the energy deposited on the target electrons relaxes via an electron–phonon coupling, leading to a thermal spike supposed to be inefficient in good electrical conductors. The second model, by Fleisher *et al* in

0953-8984/93/080995+24$07.50

1965 [3], considers that, before any electron–phonon coupling takes place, the target atoms situated along the ion path are ionized during a time long enough to undergo a Coulomb repulsion. This latter model accounts for the creation of latent tracks in most insulating materials. However, the authors claimed that this mechanism should be inoperative in electrical conductors. In this situation, the investigation of any effects induced by electronic energy loss in metallic materials appears at least as a challenge.

The first experiment where it was proposed that an electronic energy loss effect was operating in a metallic compound was the amorphization of $Pd_{80}Si_{20}$ by ^{235}U fission fragments [4]. However, in this case, both inelastic and elastic contributions had to be taken into account. The availability of high-energy heavy-ion accelerators (namely VICKSI-Berlin, GSI-Darmstadt and GANIL-Caen) to the solid state physicist community has allowed, recently, the topic to be revisited. The GeV ion beams present the advantage that the two slowing-down processes are efficiently separated, as can be seen in figure 1. In the last decade, an increasing number of unexpected experimental results has been published. In pure metals, it has been demonstrated that electronic energy loss induces either a decrease [5–7] or an enhancement [7–9] of the radiation damage efficiency. A more dramatic effect has been seen in crystalline metallic Ni_3B [10] and Ni–Zr [11] alloys: amorphization and latent track creation, which had so far been observed only in insulating materials. In amorphous materials (metallic or not), a new effect induced by $(dE/dx)_e$ has been discovered [12, 13]: a huge plastic deformation at constant volume occurs exactly as if the ion beam acted as a hammer (the sample dimensions perpendicular to the ion beam direction increase with the ion fluence, without any saturation, whereas the sample dimension parallel to it shrinks). This phenomenon has been called *growth* since the term was used for analogous dimensional changes first observed in anisotropic metals [14]. It has to be remarked that the physical origin of the two phenomena is totally different. In anisotropic crystalline metals the growth originates from an anisotropic condensation of point defects in dislocation loops whose geometry is linked to the crystallographic structure of the metals; in amorphous materials the anisotropy which causes the growth arises from the irradiation geometry and is induced by the ion electronic energy loss. In order to better understand the processes which allow the conversion of electronic excitation into atomic rearrangements, we have performed electrical resistance measurement on a $Fe_{85}B_{15}$ amorphous alloy irradiated with high-energy heavy ions. This system has been chosen since the behaviour of amorphous Fe–B alloys has already been largely studied in the case of elastic collisions induced by 2.5 MeV electrons [15], ^{10}B fission fragments [16], and low-energy H, Kr and Bi ions [17]. Preliminary experiments have shown that $(dE/dx)_e$ induces not only anisotropic dimensional variations (i.e. atomic motion) but also atomic displacements leading to a modification of the short-range order of the alloy [18–22]. In this respect, the electrical resistance R is an interesting parameter since it takes into account both intrinsic radiation-induced effects (electrical resistivity ρ) and changes of the sample dimensions (shape factor). The electronic stopping power has been varied from 5 keV nm^{-1} up to 70 keV nm^{-1} by using a set of GeV ions from Ar to U at GANIL and GSI. As the anisotropy of the effect is related to the ion beam direction, the angle of incidence of the beam with respect to the normal to the sample surface was varied from 0° to 65°. The effect of the irradiation temperature was also investigated since the observed phenomena involve both defect creation and atom migration. Finally, as the growth phenomenon is clearly related to an atomic transport process similar

to plastic deformation or creep, the effect of an external uniaxial stress, applied at low temperature during ion irradiation, was examined.

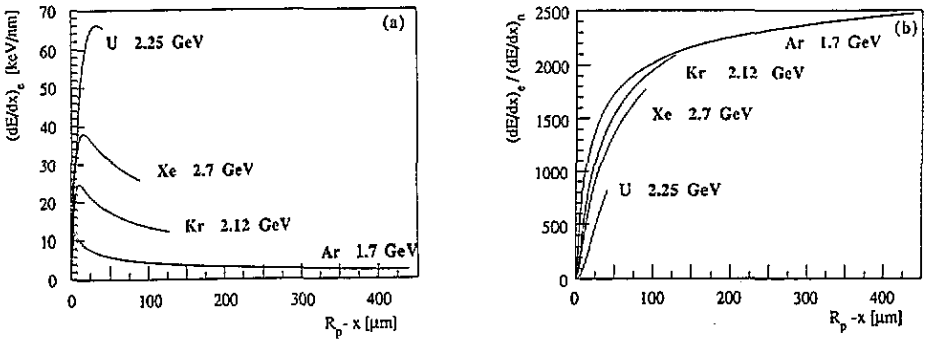

Figure 1. (*a*) The electronic energy loss of GeV heavy ions in $Fe_{85}B_{15}$ as a function of the residual ion range R_p–x where R_p is the total projected range and x is the penetration depth in the target. (*b*) The ratio between electronic and nuclear energy loss versus R_p–x for the same ion–target combinations.

The aim of this paper is: (i) to give a review of the whole set of experimental results obtained so far; (ii) to analyse the results in the framework of a phenomenological model; and (iii) to present a tentative microscopic interpretation of the reported effects.

2. *Experimental*

The samples used are amorphous $Fe_{85}B_{15}$ ribbons (1 mm wide, 21 μm thick, a few cm long) prepared by melt spinning. They were irradiated, without any structural relaxation treatment, in the IRABAT facility [23] with high-energy heavy ions (in the GeV range) at the GANIL-Caen (Ar, Kr, Mo, Xe) or GSI-Darmstadt (U) accelerators. The irradiation flux was monitored by the secondary electron emission produced by the ion beam passing through a polarized 2.5 μm thick Ta foil, and calibrated with a Faraday cup. The relative uncertainty of the ion flux is estimated to be 20%. In order to get an homogeneous irradiation over the whole sample surface, the ion beam was either magnetically swept (at GANIL) or simply defocused (at GSI).

Figure 1(*a*) shows the amount of electronic energy loss deposited onto a sample by various irradiating ions as a function of the ion residual range. As this range can be as large as a few hundred μm, the irradiation of sample stacks (including eventually Al foil energy degraders) was possible, thus showing the variation of the ion energy (and consequently the electronic energy loss) in a single experiment. In any case the overall sample stack thickness was kept small enough in order to avoid the incident ions stopping in the target. Thus, the ratio $(dE/dx)_e/(dE/dx)_n$ always remained very large (of the order of 10^3), whatever the nature of the ion and its energy (see figure 1(*b*)).

Irradiation was performed at various temperatures (20 K, 90 K, 223 K) measured by copper–constantan thermocouples soldered on the samples outside the irradiated

Table 1. Irradiation parameters: E, the mean ion energy into the sample; $(dE/dx)_e$, the ion electronic energy loss; ϕ_{max}, the fluence at the end of the irradiation; DPA_{max}, the number of displacements per atom induced by nuclear collisions at ϕ_{max}; T, the irradiation temperature; θ, the irradiation tilt angle; and σ, the uniaxial tensile stress applied to the sample during irradiation. The numbers in brackets in the first column indicate the references in which the corresponding results have been partly published.

Ion	E (GeV)	$(dE/dx)_e$ (keV nm^{-1})	ϕ_{max} (10^{13} cm^{-2})	DPA_{max} (10^{-4})	T (K)	θ (deg)	σ (MPa)
Ar							
[18]	0.54	5.4	6.5	4.4	90	0	0
Kr							
[18]	2.12	11.5	5.7	2.8	90	0	0
	1.77	12.7		3.0		0	0
	1.52	13.9		3.8		0	0
	1.23	15.6		4.7		0	0
This paper	0.48	22.4	8	14.0	90	0	0
	0.44	22.8		18.0		45	0
Mo	1.76	17.8		0.06	90	0	0
	1.68	18.0	0.08	0.06		0	0
This paper	1.26	20.8		0.09		0	0
	0.92	23.0		0.11		0	0
	0.63	25.7		0.15		0	0
Xe							
[18]	2.79	24.3	3.0	3.1	90	0	0
	2.11	27.3		3.9		0	0
	1.44	31.2		5.5		0	0
	0.64	36.6		10.8		0	0
[19]	2.79/2.78	24.3/24.4	1.9	2.0	90	0/11	0
	2.75	24.5		2.0		29/31	0
	2.68/2.66	24.7/24.9		2.0		44/48	0
	2.57/2.52	25.3/25.5		2.1		58/61	0
[20]	2.79	24.3	1.7	1.8	90	0	0
	2.79	24.3		1.8		0	600
	2.61	25.0		1.9		53	0
[21, 22]	2.79	24.3	2.4	2.5	90	0	0
	2.79	24.3		2.5		0	600
	2.73	24.6		2.5		35	0
	2.73	24.6		2.5		35	300
	2.73	24.6		2.5		35	600
	2.61	25.0		2.6		53	0
	2.61	25.0		2.6		53	300
	2.61	25.0		2.6		53	600
[21, 22]	2.79	24.3	2.4	2.5	223	0	0
	2.73	24.6		2.5		35	0
	2.73	24.6		2.5		35	300
	2.61	25.0		2.6		53	0
	2.61	25.0		2.6		53	300
	2.61	25.0		2.6		53	600
This paper	2.79	24.3	3.6	3.7	20	0	0
	2.73	24.6		3.8		35	0
	2.69	24.8		3.9		45	0
	2.45	25.8		4.2		65	0
U	2.25	65.1	1.0	1.7	90	0	0
This paper	1.96	65.8		1.9		32	0
	1.72	66.7		2.0		55	0

area. The samples were cooled down by a He exchange gas at a pressure of around 100 mbar. The ion flux was generally lower than 10^9 ion cm^{-2} s^{-1} in order to keep the sample heating during irradiation below 10 K. Throughout the experiment, the radiation damage created inside the target was monitored by *in situ* electrical resistance measurements performed during the beam stops at a reference temperature (11 K, 80 K, 220 K), by using a conventional DC four-point technique with a resolution better than 10^{-4}. The samples were mounted on the irradiation set-up at various tilt angles θ (from 0° to 65°) between the beam axis and the normal to the sample foil (the direction of the DC measurement current was along the sample length, the sample width always remained perpendicular to the beam axis, as shown in figure 2). The uncertainty in the tilt angle may reach 5° at the end of the irradiation, due to radiation-induced sample deformation. To minimize the growth-induced tilt angle variation, the samples were generally slightly tightened by means of a soft spring, leading to a residual stress lower than 5 MPa. The effect of an external uniaxial tensile stress (300 MPa or 600 MPa) was also investigated. The stress was applied by means of a spring and calibrated by comparison with elastic deformations induced in the samples by different weights. The relative uncertainty on the applied stress is estimated to be about 20%. Moreover, the stress changes, due to the dimensional variations of the samples during irradiation, were not taken into account. Without irradiation, the stability of the electrical resistance of the samples was checked at the irradiation temperature. No drift was observed for the stressed samples, thus indicating that no creep occurred without irradiation. Annealing experiments were also performed at the end of the irradiation for some of the samples, at a constant heating rate ~ 1 K min^{-1}, from the irradiation temperature up to room temperature. Table 1 summarizes the experimental conditions.

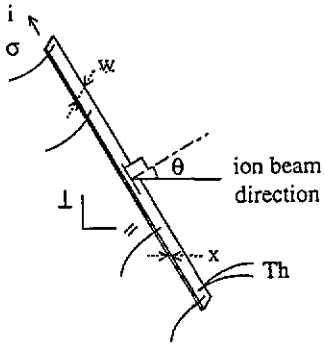

Figure 2. A schematic representation of the geometry used for the irradiation of ribbons (width w, thickness along the ion beam direction x) tilted at an angle θ with respect to the ion beam direction: i, the DC current; σ, the stress applied to the ribbon; and Th indicates the position of the copper–constantan thermocouple.

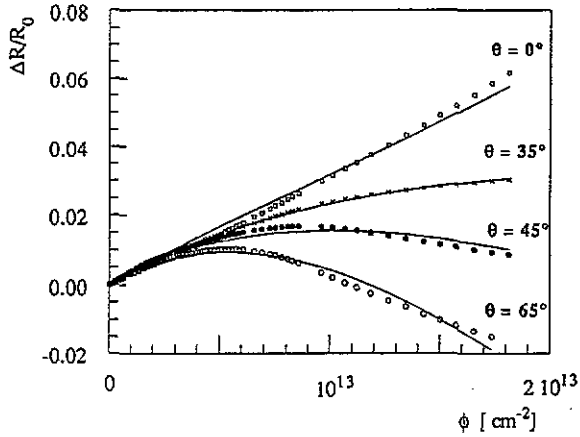

Figure 3. The ion fluence dependence of the electrical resistance of $Fe_{85}B_{15}$ ribbons irradiated at 20 K with 2.8 GeV Xe ions in the geometry schematized in figure 2. The full curves represent best fits to the experimental data, using equation (5).

3. Results and analysis

A typical curve representing the variation of $\Delta R/R_0$ of the amorphous $Fe_{85}B_{15}$ ribbons with the ion irradiation fluence for different tilting orientations θ is displayed in figure 3; ΔR is the electrical resistance increment and R_0 the initial value of R. In order to account for the behaviour of the ribbon resistance exhibited in the figure, a two-hit phenomenological model has been developed. We will first summarize this model. Then, the experimental data obtained for the amorphous $Fe_{85}B_{15}$ alloy will be analysed in the framework of this model.

3.1. Two-hit model and analysis procedure

Figure 3 shows that the increase of the electrical resistance of the irradiated ribbons is independent of the angle θ at low fluence. This result indicates that only electrical resistivity increase and shape factor variation independent of the incident beam direction occur. The resistivity increase can be attributed to disorder creation along the path of the incoming ions with a cross section s_d and an associated relative resistivity variation r_d. This disorder creation can induce an isotropic swelling of the irradiated target. However, such a swelling cannot be taken into account by the electrical resistance measurements presented in this paper due to its isotropic behaviour. The shape factor variations induced by the swelling are nevertheless certainly much smaller than those arising from the growth phenomenon [13] and are neglected in the analysis of the resistance data.

As the irradiation fluence increases, the curves of figure 3 are split according to the value of the tilt angle θ, in agreement with the assumption that anisotropic dimensional changes occur. The existence of an incubation fluence for the occurrence of the anisotropic sample growth suggests a two-hit phenomenon: an ion passing in the vicinity of an already disordered region is supposed to induce anisotropic atomic movements, which cause an anisotropic macroscopic deformation of the irradiated target. A cross section s_g is attributed to this second-hit process and the relative resistivity variation of a twice-hit region is r_g. Figure 4 gives a schematic representation of the above hypotheses. The variation with the irradiation fluence ϕ of the fraction c_d and c_g of disordered and 'grown' regions is then represented by the following system of differential equations:

$$dc_d/d\phi = s_d(1 - c_d) - s_g c_d \tag{1a}$$

$$dc_g/d\phi = s_g c_d - s_d c_g. \tag{1b}$$

The change in dimensions of the sample is accounted for by the first term $(s_g c_d)$ of the right-hand side of equation (1*b*). The second term $(-s_d c_g)$ assumes that a 'grown' region can be disordered by a subsequent ion impact in the same manner as a virgin one.

In the course of irradiation, the target is composed of undamaged, damaged and 'grown' regions. It can be assumed that the total resistivity ρ of the irradiated alloy is the weighted sum of the resistivities of these different types of regions since the whole relative resistivity change is small compared with unity. Then it follows that

$$(1/\rho_0)d\rho/d\phi = r_d dc_d/d\phi + r_g dc_g/d\phi \tag{2}$$

where ρ_0 is the resistivity of the virgin material.

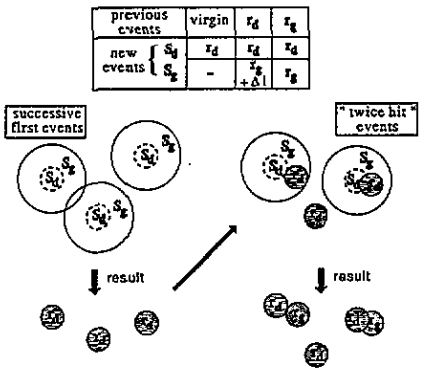

Figure 4. A schematic representation of the hypotheses made for the development of the phenomenological model used to account for the electrical resistance data presented in figure 3.

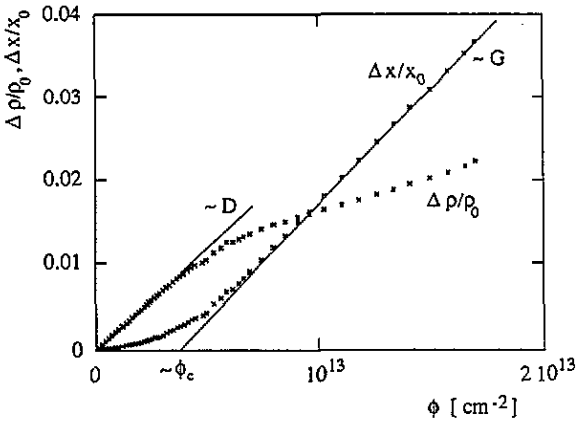

Figure 5. The ion fluence dependence of the electrical resistivity and of the length of $Fe_{85}B_{15}$ ribbons irradiated at 20 K with 2.8 GeV Xe ions. The curves are deduced by a deconvolution of the data presented in figure 3 according to equation (4). The physical meaning of the parameters D, G, and ϕ_c is shown.

In order to reproduce the variations with the irradiation fluence of the ribbon dimension x along the ion beam direction (see figure 2), it is necessary to introduce a parameter η_0 which accounts for the efficiency of the ion-induced atomic movements creating a macroscopic observable growth:

$$-(1/x_0)\mathrm{d}x/\mathrm{d}\phi = \eta_0 s_g c_d. \tag{3}$$

The parameter η_0 may vary between 0 (isotropy) and 1 (for the case where all the atoms contained in the overlap volume of a previously damaged zone with a cylinder of section s_g contribute with one atomic volume to the anisotropic dimensional change of the sample).

For a tilt angle θ between the ion beam direction and the normal to the sample surface, the resistance variation can be written, considering that the growth occurs at a constant volume [12, 24], as

$$\Delta R(\phi)/R_0 = \Delta\rho(\phi)/\rho_0 - (\Delta x(\phi)/x_0)(1 - 3\sin^2\theta). \tag{4}$$

Integrating equations (1) and combining equations (2) to (4) lead to the general equation describing the variation of the ribbon resistance with ion fluence:

$$\frac{\Delta R}{R_0} = r_d s_d \left(\frac{1-\exp[-(s_d+s_g)\phi]}{s_d+s_g}\right) + r_g\left(1-\exp[-(s_d\phi)] - \frac{s_d}{s_d+s_g}\left\{1-\exp[-(s_d+s_g)\phi]\right\}\right) + \eta\frac{s_d s_g}{s_d+s_g}\left(\phi - \frac{1-\exp[-(s_d+s_g)\phi]}{s_d+s_g}\right) \tag{5}$$

where

$$\eta = \eta_0(1 - 3\sin^2\theta). \tag{6}$$

Equation (5) reproduces the essential features of the usual behaviour of amorphous alloys submitted to high-energy ion irradiation [12, 13, 18, 19] and has been successfully applied to fit the data obtained on $Ni_{75}B_{25}$ amorphous alloys irradiated with 3 GeV heavy ions [25, 26]. The first two terms on the right-hand side of this equation represent the damage and the growth contributions in the alloy resistivity variation, respectively, whereas the third term accounts for the growth contribution to the variation of the sample shape factor.

At the very beginning of the irradiation ($(s_d + s_g)\phi \ll 1$), equation (5) reduces to

$$(\Delta R/R_0)|_0 = D\phi \tag{7}$$

where $D = r_d s_d$ is the initial rate of the alloy resistivity increase. At very high fluences ($s_d\phi \gg 1$), equation (5) becomes

$$(\Delta R/R_0)|_\infty \simeq (r_d s_d + r_g s_g)/(s_d + s_g) + \eta[s_d s_g/(s_d + s_g)][\phi - 1/(s_d + s_g)] \tag{8}$$

which can be rewritten as

$$(\Delta R/R_0)|_\infty = (\Delta\rho/\rho_0)|_\infty + G(\phi - \phi_c) \tag{9}$$

where G is the final rate of the sample dimensional variation and ϕ_c is the incubation fluence.

This model involves five independent parameters: r_d, s_d, r_g, s_g and η_0. Unfortunately, it is generally impossible to extract the five parameters with a high degree of confidence from a fit of equation (5) to experimental electrical resistance data. However, four parameters: D, G, ϕ_c and $(\Delta\rho/\rho_0)|_\infty$ enter the asymptotic equations (7) and (9). It is possible to graphically determine three of them (D, G, ϕ_c) in the cases where data have been recorded at different tilt angles θ (i.e. for the curves presented in figure 3). The physical meaning of D, G and ϕ_c is indicated in figure 5 where $\Delta\rho/\rho_0$ and $\Delta x/x_0$ have been deduced from the curves presented in figure 3 according to equation (4). It has to be noted that, as only one tilt angle is used (a classical case of irradiation at normal incidence), only D and G can be graphically determined. The remaining parameter ϕ_c is then extracted by choosing an appropriate value for r_d (see section 4.1), r_g being left free. As can be seen in figure 3 and in the figures presented hereafter, a good agreement is generally obtained between the fits and experimental data.

3.2. Data analysis

In this section, the respective roles of elastic and inelastic collisions will be discussed. The influence of the different irradiation parameters: the tilt angle θ, the irradiation temperature T, and the applied tensile stress σ on the structural modifications induced by electronic energy loss in amorphous $Fe_{85}B_{15}$ will then be considered. Finally, the results obtained during annealing of the irradiated samples up to room temperature will be presented.

3.2.1. Role of elastic collisions and electronic energy loss. Although the ratio $(dE/dx)_e/(dE/dx)_n$ is always very high in the experiments reported here (see figure 1(*b*)), the influence of elastic collisions on the structural modifications (damage creation and growth) induced by swift-heavy-ion irradiation cannot be excluded *a priori*. Table 2 collects some data: the elastic displacement cross section σ_d, the mean number of displaced atoms per primary event $\bar{\nu}$, and the mean free path between two primary events λ, related to the atomic displacements created by nuclear energy loss in amorphous Fe–B alloys irradiated with various particles. This table shows that swift heavy ions induce on average few atomic displacements per primary collision, separated by distances much higher than the alloy interatomic spacing, while low-energy heavy ions (0.27 MeV Bi) create dense displacement cascades. The consequence is that, as far as elastic collisions are concerned, swift heavy ions induce events close to those due to electrons, i.e. they essentially create isolated point defects. Nevertheless, it must be pointed out that, although the low-energy transfers dominate, a few high-energy primary knock-on atoms can be responsible for the creation of dense cascades. Anyway, table 1 indicates that the total number of DPA (displacements per atom) reached in the present experiments (lower than 10^{-3}) cannot account for the large radiation damage effects reported here.

Table 2. Calculated damage parameters: σ_d, the displacement cross section for the nuclear collisions; $\bar{\nu}$, the mean number of displaced atoms per collision; λ, the mean free path between two collisions.

Particle	Mean energy (MeV)	Target	σ_d (cm^2)	$\bar{\nu}$	λ (nm)	Ref.
e	2.5	$Fe_{75}B_{25}$	1×10^{-22}	1.1	10^6	[15]
Bi	0.27	$Fe_{75}B_{25}$	1.4×10^{-14}	51	0.35	[17]
Ar	1.7×10^3	$Fe_{85}B_{15}$	7.7×10^{-19}	7.2	10^3	This paper
U	2×10^3	$Fe_{85}B_{15}$	2×10^{-17}	7	30	This paper

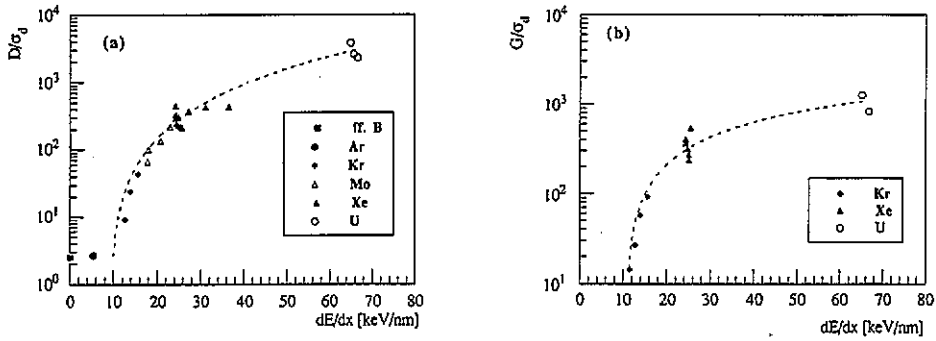

Figure 6. The ratio of the relative electrical resistance variation to the calculated number of elastic DPA as a function of the average electronic energy loss for $Fe_{85}B_{15}$ irradiated with various high-energy heavy ions: (*a*) the beginning of the irradiation; (*b*) the end of the irradiation. The broken curve serves only as a guide to the eye.

Another way to attest that nuclear collisions have a negligible effect on the structural modifications induced in amorphous Fe–B alloys irradiated with high-energy

heavy ions is to plot as a function of $(dE/dx)_e$ the variation rate of the relative resistance of the irradiated ribbons, normalized to the calculated number of DPA created by the ion beam. Figures 6(*a*) and 6(*b*) respectively present the results of such a plot at the beginning (i.e. as the parameter D dominates the damage process as shown in equation (7)) and at the end (i.e. as G dominates the growth process as shown in equation (9)) of the irradiation. The figure illustrates (i) the existence of a $(dE/dx)_e$ threshold for the damaging and growth processes; and (ii) the negligible influence of elastic collisions on the observed phenomena above this threshold.

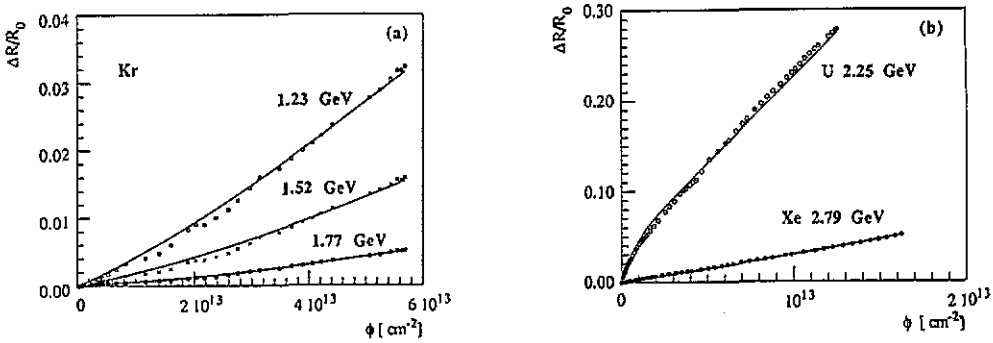

Figure 7. The ion fluence dependence of the relative electrical resistance of $Fe_{85}B_{15}$ ribbons irradiated at 90 K with various high-energy heavy ions. The full curves represent the best fits to experimental data using equation (5).

The effect of the ion electronic energy loss on $\Delta R/R_0$ is illustrated in figure 7 where the data relative to a great variety of irradiating ions are presented. Figure 8 shows the variation with $(dE/dx)_e$ of the parameters deduced from the whole set of data recorded at 80 K (see table 1) with the procedure described in section 3.1. It is worth noting that the initial disordering rate D, the growth rate G and the incubation fluence ϕ_c follow a supra-linear dependence on $(dE/dx)_e$. A variation of three orders of magnitude is observed as the ion electronic energy loss is multiplied by a factor of 10.

3.2.2. Role of the tilt angle. A study of the influence of the tilt angle θ allows a more specific investigation of the anisotropy of the irradiation-induced growth, i.e. to verify the validity of equations (4) and (6). Figure 3 presents the case of 20 K Xe irradiation with four values of θ ranging from 0 to 65°. At irradiation fluences higher than the incubation fluence $\phi_c \sim 5 \times 10^{12}$ ions cm^{-2}, the electrical resistance variation of the irradiated ribbon, due to the anisotropic dimensional variation (growth), (i) is very small for $\theta \sim \theta_c$ ($\theta_c = 35.3°$), (ii) increases for $\theta < \theta_c$, and (iii) decreases for $\theta > \theta_c$, as expected from equation (4). At irradiation fluences lower than ϕ_c, no tilt angle dependence is observed since only changes of the ribbon resistivity are supposed to occur. These observations are confirmed by the data presented in figure 9 where the initial disordering rate D and the growth rate G are plotted as a function of $\sin^2\theta$.

3.2.3. Role of the irradiation temperature. A better understanding of the microscopic mechanisms leading to the structural modifications observed in swift-heavy-ion-irradiated alloys is obtained through a study of the temperature dependence of the

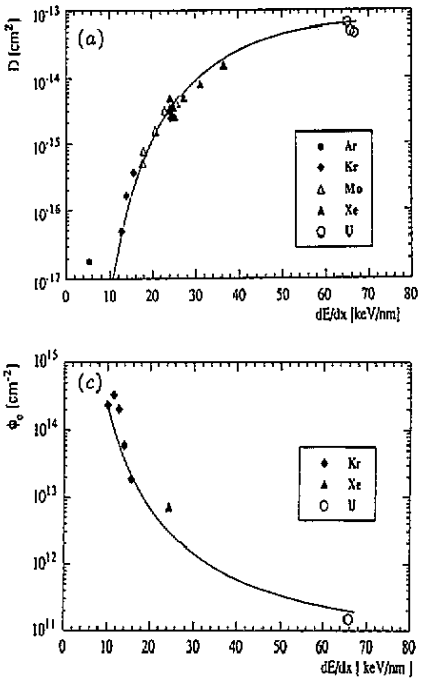

Figure 8. The electronic energy loss dependence of D (*a*), G (*b*), and ϕ_c (*c*) extracted from the fits to experimental data for $Fe_{85}B_{15}$ ribbons irradiated with various high-energy heavy ions. The full curves are best polynomial fits to the data.

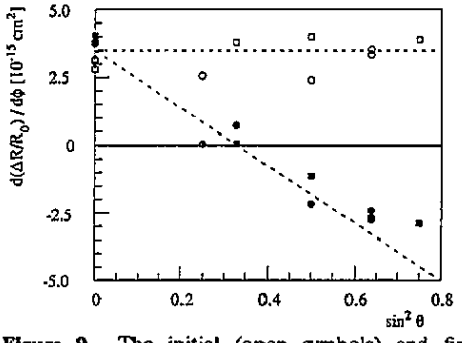

Figure 9. The initial (open symbols) and final (full symbols) relative resistance variation rate as a function of $\sin^2\theta$ for $Fe_{85}B_{15}$ ribbons irradiated at 90 K (circles) and 20 K (squares) with 2.8 GeV Xe ions.

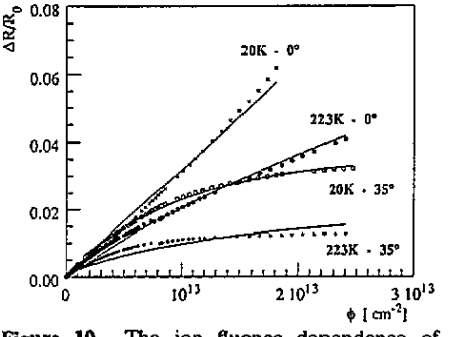

Figure 10. The ion fluence dependence of the relative electrical resistance of $Fe_{85}B_{15}$ ribbons irradiated at 20 K and 223 K with 2.8 GeV Xe ions at tilt angles of 0° and 35°. The full curves represent best fits to experimental data using equation (5).

effects induced by electronic excitation. The influence of the irradiation temperature (20 K, 90 K, 223 K) was recently studied in the case of Xe irradiation. Since no difference was detected within the limit of the experimental uncertainties between 20 K and 90 K, the data recorded at 90 K were omitted in figure 10. It is quite clear that both the saturation resistivity (as seen for the 35° tilted ribbon for which $\eta \sim 0$ in equation (5)) and the growth rate G strongly decrease as the irradiation temperature increases. The latter result is in agreement with the experiments performed on amorphous Pd–Si alloys [12, 24]. Moreover figure 10 indicates that the initial disordering rate D is independent of the temperature; a more careful

analysis of the data shows that the ratio G/ϕ_c is also roughly independent of T. On the contrary ϕ_c decreases from 5×10^{12} cm^{-2} for $T \leqslant 90$ K down to 10^{12} cm^{-2} for $T = 223$ K. This implies that s_g increases as the temperature increases.

3.2.4. Role of internal and external stresses. The huge anisotropic growth observed in amorphous ribbons irradiated with high-energy heavy ions implies both an increase of the atomic mobility in the irradiated region and the presence of a stress induced by irradiation. The application of an external uniaxial tensile stress to the ribbon during irradiation may then serve the purpose of determining the order of magnitude of the irradiation-induced internal stress [20–22]. The external applied stress was varied from 0 to 600 MPa in the case of irradiation with a Xe ion beam. Figure 11 presents the results recorded at 80 K for three different tilt angles. It must be emphasized that even at the end of irradiation, as the damage level saturates, no drift of the dimensional variations was observed out of irradiation. The curves corresponding to the stressed samples present the same qualitative features as those corresponding to the unstressed samples above an incubation fluence; the relative resistance increases linearly with the ion fluence without any saturation, due to a variation of the sample dimensions. This figure exhibits the huge effect of the applied stress on the resistance variation: for normal incidence the value of $\Delta R/R_0$ is multiplied by a factor of 20 at the end of irradiation; for a tilt angle of 53° the variation of $\Delta R/R_0$ is inverted. Thus, this phenomenon can be regarded as a creep induced by electronic excitation†.

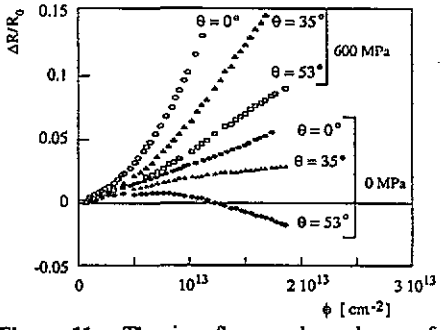

Figure 11. The ion fluence dependence of the relative electrical resistance of $Fe_{85}B_{15}$ ribbons irradiated at 90 K for different tilt angles θ between the ion beam and the normal to the sample surface: full symbols, no applied stress; open symbols, 600 MPa uniaxial tensile stress applied to the samples.

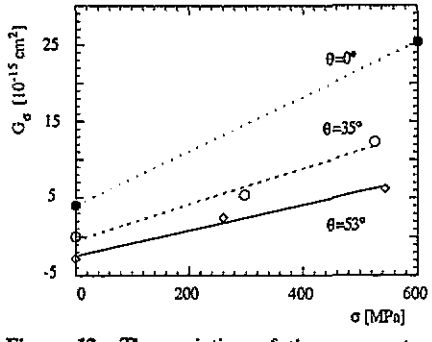

Figure 12. The variation of the apparent growth rate G_σ (see text) as a function of the applied uniaxial tensile stress for three different tilt angles θ.

The application of a uniaxial tensile stress splits the degeneracy of the ribbon expansion perpendicularly to the ion beam direction. The growth phenomenon can no longer be described by the parameter η alone. Two parameters $\eta_{\|}$ and $\eta_{\perp}$ (the subscripts $\|$ and $\perp$ respectively correspond to the directions indicated in figure 2) are

† The fact that elastic collisions play no role in the observed 'irradiation-assisted creep' was confirmed by length measurements performed on two amorphous $Fe_{85}B_{15}$ ribbons submitted respectively to a 0 and 600 MPa tensile stress and irradiated at 20 K with 2.5 MeV electrons. The results show no difference between the two samples.

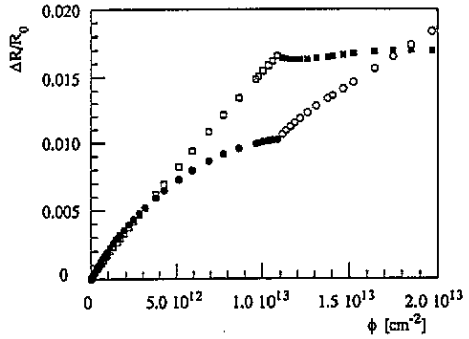

Figure 13. The ion fluence dependence of the relative electrical resistance of two $Fe_{85}B_{15}$ ribbons irradiated at $\theta = 0°$ (open symbols) and $\theta = 45°$ (full symbols). One of the samples (squares) was irradiated at 0° up to a fluence of 1.1×10^{13} cm^{-2} and then at 45°. The other sample (circles) was irradiated at 45° up to a fluence of 1.1×10^{13} cm^{-2} and then at 0°.

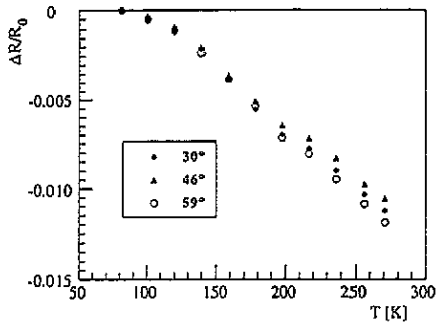

Figure 14. The annealing curves for three $Fe_{85}B_{15}$ ribbons irradiated at 90 K with 2.8 GeV Xe ions at various tilt angles θ. R is the resistance at the end of the irradiation.

thus required to account for the observed effects. Equation (6) can then be rewritten as

$$\eta(\theta, \sigma) = 2[\eta_\perp(\theta, \sigma)\cos^2\theta + \eta_\parallel(\theta, \sigma)\sin^2\theta]. \tag{10}$$

In this equation $\eta_\perp$ and $\eta_\parallel$ generally depend on both σ and θ. It can be remarked that without external stress $\eta_\perp$ and $\eta_\parallel$ are related by

$$2\eta_\perp + \eta_\parallel = 0. \tag{11}$$

which expresses the fact that the growth occurs at a constant volume. Moreover, the parameter η_0 introduced in equation (3) is, according to this notation, nothing else but $2\eta_\perp(0,0)$. It is possible to deduce a value for the apparent growth factor in the presence of the external stress, G_σ, from the resistance variation at the end of irradiation (see equation (9)). Unfortunately this value does not allow a full characterization of the dimensional variation of the sample, since equation (10) shows that the anisotropy parameter is split in this case into two components. Figure 12 presents the variation of G_σ with σ for different values of θ. This variation is roughly linear whatever the value of θ. From these results, a value ~ 100 MPa for the internal stress induced by electronic excitation in the wake of the incident ion can be derived (see section 4.4).

The problem that remains to be understood is the microscopic origin of the internal stress. In the framework of the two-hit model developed above, this stress can be either due to the presence of the initially damaged region (cross section s_d), or linked to the second hit (cross section s_g). An experiment has allowed us to enlighten this puzzling situation: an irradiation of two ribbons with initial tilt angles $\theta = 0°$ and 45° which are reversed to $\theta = 45°$ and 0°, respectively, at a given irradiation fluence. Figure 13 presents the result of this experiment performed with Kr ions. The data, which exhibit a sharp change in the slope of the electrical resistance variation as the tilt angles are changed, demonstrate that the second hit is entirely responsible for the anisotropy of the atomic movements leading to the sample growth.

3.2.5. Annealing behaviour. Some of the samples irradiated at 90 K with Kr and Xe ions were slowly (~ 1 K min^{-1}) annealed up to room temperature and their electrical resistance measured. Figure 14 presents a typical annealing curve for various values of the tilt angle θ. It can be seen that the annealing behaviour of the ribbons is independent of θ and can then be interpreted in terms of a resistivity decrease only. Moreover, the data are quite similar to those recorded after an irradiation with 2.5 MeV electrons [15].

4. Discussion

We have shown that irradiation of amorphous $Fe_{85}B_{15}$ with swift heavy ions leads to two types of atomic rearrangements essentially induced by $(dE/dx)_e$: (i) for ion electronic stopping powers higher than a threshold value ~ 10 keV nm^{-1}, a modification of the alloy short-range order from the very beginning of the irradiation; (ii) an anisotropic sample growth starting above an incubation fluence with a growth rate which depends on the value of both $(dE/dx)_e$ and the irradiation temperature. As a uniaxial stress is applied to the sample during irradiation, the dimensional changes are strongly modified and a huge radiation-induced stress-biased growth appears.

We have proposed a phenomenological model which accounts for the electrical resistance variations reported in this paper. The first part of the discussion is devoted to the determination of the physical parameters from the quantities directly available from the experimental data. A discussion of the importance of the metallic character and of the structure of the irradiated alloy, of the role of the electronic stopping power, of the irradiation temperature, and of the applied stress on the damage process is then presented.

4.1. Determination of the physical parameters

The microscopic processes involved in the electronic-excitation-induced atomic rearrangements occurring in amorphous $Fe_{85}B_{15}$ are mainly accounted for by the parameters s_d, s_g and η_0 involved in the phenomenological model. In fact, as already discussed in section 3.1, the experimental data provide an unambiguous determination of three quantities only: D, G and ϕ_c, which are combinations of four (r_d, s_d, s_g, η_0) of the five parameters of the model. As a matter of fact, the relative resistivity of the grown regions r_g does not appear in the expressions for D, G and ϕ_c. On the other hand, the model implicitly assumes that the degree of damage in the disordered regions is saturated, since it was supposed in the derivation of equations (1) that (i) a disordering event (cross section s_d) occurring in a disordered region does not change the relative resistivity r_d and (ii) a grown region behaves from the point of view of the disordering process as a virgin one. A reasonable hypothesis is then to consider that r_d is an intrinsic value of the investigated alloy which is independent of both the ion stopping power and the irradiation temperature. In this respect, it has to be noted that in $Fe_{76}B_{24}$ thin films irradiated with several hundred keV H, Kr and Bi ions [17], the value of the relative increase of the film resistivity at saturation is the same whatever the projectile used, i.e. whatever the type of defects (Frenkel pair-type or dense displacement cascades) created during irradiation. The alloy under investigation here is unfortunately not of exactly the same composition as those irradiated with low-energy ions ($Fe_{76}B_{24}$), ^{10}B fission fragments or 2.5 MeV electrons ($Fe_{75}B_{25}$ and

$Fe_{80}B_{20}$) [15, 16]. Nevertheless an extrapolation of the previous results to the present case certainly provides a good estimation of the saturation value of the resistivity of a disordered region: $r_d = 0.04$. Figure 15 presents the variations of s_d, s_g and η_0 with the ion electronic stopping power, obtained from the quantities D, G and ϕ_c, by taking for r_d the value estimated above.

4.2. Disorder creation

Up until now, we have always considered that irradiation induces changes in the short-range order of the amorphous packing but does not lead to any amorphous-to-crystalline phase transformation. In fact, no sign of crystallization has been detected in any of our samples: the temperature coefficient of the alloy resistivity, which is very sensitive to an incipient crystallization, was always found to be nearly the same after irradiation as it was before. This result is not surprising in the light of other experiments which have shown that, at low temperature, a similar metal–metalloid system (Ni_3B) undergoes a crystalline-to-amorphous transition induced by electronic excitation [10, 26]. Furthermore, the only evidence for crystallization of an amorphous material (metallic or not) driven by $(dE/dx)_e$ concerns room-temperature irradiation of very thin films of Si and Ge [27] and W–Si multilayers [28]. The specific behaviour of the thin films could be ascribed to the role of both the temperature and the surface (the presence of a crystalline substrate) or interface (the role of a mixing effect) in the nucleation and growth of a crystalline phase.

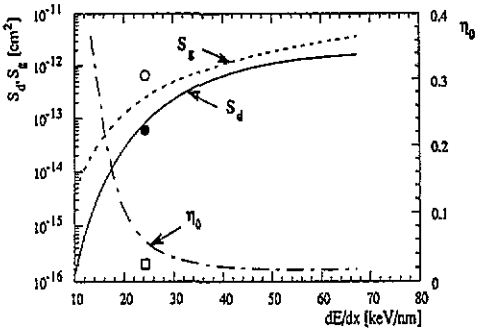

Figure 15. The ion electronic energy loss dependence of s_d, s_g and η_0. The curves are deduced from those presented in figure 8 for the data recorded at 80 K, assuming that $r_d = 0.04$. The symbols refer to experimental data recorded at 220 K.

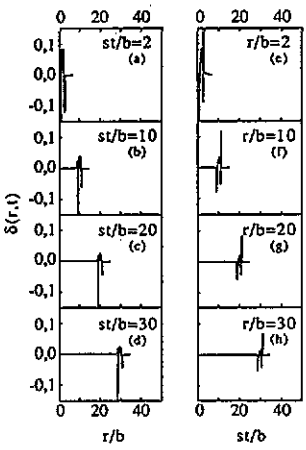

Figure 16. The variation of the dilatation $\delta(r, t)$ (see text) versus r/b for a given value of the time t ((a)–(d)) and versus st/b for a given value of r ((e)–(h)).

The results previously obtained in amorphous Fe–B alloys irradiated with low-energy ions or electrons, which induce damage creation by elastic collisions, were interpreted in terms of Frenkel pair-type defects characterized by an intrinsic relative resistivity ($\rho_{FP}/\rho_0 = 2.5$) and a spontaneous recombination volume ($v_0 = 60$ atomic volume) [15]. The saturation level of the created damage then corresponds to a defect concentration of $1/v_0 = 1.7 \times 10^{-2}$ and to a relative resistivity increase

$r_d = (\rho_{FP}/\rho_0)v_0 = 0.04$. Now, the relevant question is: are the defects created in $Fe_{85}B_{15}$ by electronic excitation similar to those created by elastic displacements? A hint about this problem can be provided by considering the results obtained after the annealing of the irradiated samples up to room temperature: the recovery was shown to be independent of the tilt angle θ and similar to the one obtained after irradiation with electrons. The former result indicates that the shape factor remains constant during annealing: the deformation induced by the ion beam does not anneal out since only the resistivity increase is recovered. The latter result provides an indication that similar defects are annealed out (and thus created) in the case of both electron and swift-heavy-ion irradiation. This observation is interesting owing to the knowledge of the type of damage expected to be created by electronic excitation in amorphous metallic compounds, which could be identical to that induced by electron irradiation. However, this knowledge is not essential for the interpretation of our experimental data since the only hypothesis required is the value of the relative resistivity r_d of a disordered region.

The variation of s_d with the ion electronic energy lost exhibited in figure 15 shows an apparent $(dE/dx)_e$ threshold $\sim$ 10 keV nm^{-1} and, above this value, a supra-linear dependence (an increase of three orders of magnitude as $(dE/dx)_e$ increases by a factor less than 10). Such a threshold was commonly observed for track formation in insulators irradiated by swift heavy ions [29–31] and also very recently in a number of crystalline metallic alloys [11, 32] in which electron microscopy observations have shown the presence of continuous amorphous cylinders. It may then be assumed that the disordered regions created in $Fe_{85}B_{15}$ by swift-heavy-ion irradiation consist of cylindrical 'tracks' of radius equal to $(s_d/\pi)^{1/2}$. In a $(dE/dx)_e$ range of 20–70 keV nm^{-1} the calculated track radii vary between 1.5 and 7 nm. Values of track radii have up until now not been available in amorphous systems. A direct comparison of the damage sensitivity to high $(dE/dx)_e$ is then impossible between amorphous metals and amorphous insulators. Nevertheless, the radii of the disordered regions obtained in the present experiments are close to the amorphous track radii observed in crystalline inorganic insulators or metals irradiated under similar conditions [11, 30, 32–34]. The low values for s_d obtained near the $(dE/dx)_e$ threshold of 10 keV nm^{-1} provide meaningless values of the track radii ($\sim$ 0.18 nm) if continuous cylinders are assumed. The disordered regions in this low $(dE/dx)_e$ regime then certainly consist of discontinuous damage trails all along the ion path. It must also be pointed out that near the $(dE/dx)_e$ threshold elastic collision events play a role which can certainly not be neglected.

A change in the irradiation temperature from 20 K to 223 K brings no major variation of s_d (see figure 15). This result is consistent with the weak amount of recovery ($< 30\%$) obtained at 220 K in annealing experiments performed on Fe–B alloys irradiated with high- (see figure 14) as well as with low- [17] energy heavy ions.

Figure 6 has allowed us to demonstrate that $(dE/dx)_e$ plays a major role in the disordering process of $Fe_{85}B_{15}$ irradiated with swift heavy ions. Moreover this figure exhibits the huge ratio ($\sim 10^3$) existing between the damage efficiency (D/σ_d) measured for a $(dE/dx)_e$ value of 70 keV nm^{-1} (U irradiation) and well below the $(dE/dx)_e$ threshold. Such a value excludes *a priori* a consideration of the role of $(dE/dx)_e$ as an enhancement of the elastic collision cross section. With this hypothesis an increase of σ_d by almost three orders of magnitude would be deduced since the same defect resistivity has been assumed. This increase of σ_d could then only be accounted for by a $(dE/dx)_e$-induced decrease of the elastic displacement

threshold energy to a meaningless value of some tens of meV. On the other hand, the damage efficiency increase is two orders of magnitude higher in the case of amorphous alloys ($Fe_{85}B_{15}$ and $N_{75}B_{15}$ [25, 26]) than in the case of pure crystalline metals [7–9]. This comparison clearly stresses the major role played by the amorphous structure to accommodate more easily electronic-excitation-induced damage.

It is of primary interest to establish an energetic balance of the damage process by electronic energy loss. For this purpose, the ratio ϵ between the energy stored in disordered regions of the irradiated target and the corresponding amount of energy loss by the incident projectiles in the host electronic system may be used. The value of ϵ is equal to $s_d \Delta H_s N/(dE/dx)_e$, where N is the target atomic density and ΔH_s the amount of energy stored per atom in a damaged zone. Although no direct estimate of the stored energy is possible, a comparison can be made between the energy released during the structural relaxation of amorphous alloys and the energy stored in a disordered track (the resistivity variations involved in both processes are comparable since a relative decrease of the resistivity of 6×10^{-2} is measured during the heating of an as-quenched $Fe_{80}B_{20}$ sample up to 620 K [35]). In Fe–Ni-based metal–metalloid alloys the relaxation enthalpy measured during the heating of an as-quenched sample up to the glass transition temperature or up to the onset of crystallization varies from 2×10^{-3} to 10^{-2} eV/at depending on the samples [36]. In $Fe_{78}B_{13}Si_9$ alloys the relaxation enthalpy is equal to 1.5×10^{-2} eV/at [37]. Taking this latter value as a typical order of magnitude for ΔH_s leads to $\epsilon = 3.7 \times 10^{-3}$ in the case of U irradiation ($(dE/dx)_e = 70$ keV nm^{-1}) and 5.5×10^{-5} in the case of Kr irradiation ($(dE/dx)_e = 16$ keV nm^{-1}). Although the effects induced by electronic energy loss in amorphous metallic alloys are dramatic, these results indicate that only a very small part of the energy deposited by the incident ion beam is stored in disordered regions, as is frequently observed for the radiolysis of inorganic insulators [38].

4.3. Atomic motion

Atomic motion leading to macroscopic dimensional variations becomes significant above an incubation fluence ($\phi_c = 1/(s_d + s_g)$) at which the saturation of the sample resistivity is largely in progress ($c_d(\phi_c) = 0.63 c_d(\phi_\infty)$ from equation (1)). On the other hand, the experimental results indicate that the incubation fluence decreases as the ion stopping power increases.

The number of atoms per incident ion and over an interatomic distance which participate in the anisotropic growth process can be estimated by the equation

$$n_g = 2G_0 N^{2/3} \tag{12}$$

where $G_0 = G/(1 - 3\sin^2\theta)$. In fact, this quantity is a lower limit of the number of atoms removed from their initial atomic site per atomic layer, since the atomic motion is generally not fully anisotropic (i.e. the parameter η_0 is always < 1 as verified in figure 15). The value of n_g varies from 0.2 to 80 for irradiation with Kr (10 keV nm^{-1}) and U (65 keV nm^{-1}) ions, respectively.

Figure 15 shows that s_g and s_d are both of the same order of magnitude and vary in the same way with the ion electronic stopping power. Moreover, the $(dE/dx)_e$ threshold for the growth process is not higher than that seen for the damage process. This indicates either that the same threshold energy is required for both processes

or that the threshold energy for the growth phenomenon is lower, this latter process being triggered by disorder creation. Figure 15 indicates that η_0 decreases as the electronic energy loss increases. Such a result might be surprising owing to the fact that the growth rate increases as $(dE/dx)_e$ increases. However, it has to be re-stated that the number of atoms involved in the growth phenomenon vary as the product $\eta_0 s_g$, which was found to increase as $(dE/dx)_e$ increases†.

As the irradiation temperature increases, both ϕ_c and G decrease. The decrease of ϕ_c is mostly due to the variation of s_g, since s_d has been shown to be nearly temperature independent. On the other hand, the decrease of η_0 overwhelms the increase of s_g, thus leading to the observed decrease of the growth efficiency. As a matter of fact, an increase of the irradiation temperature serves the double purpose of increasing and randomizing the atomic motion.

In the model developed earlier by Klaumünzer and co-workers [13, 39] to account for the growth phenomenon observed in a large variety of amorphous materials irradiated with high-energy heavy ions, the pertinent parameters are the free volume initially present in the irradiated target, the elastic collision cross section and the ion electronic stopping power. In the following we will discuss the role of the two former parameters in the irradiation behaviour of $Fe_{85}B_{15}$ in the framework of the phenomenological description presented above. As has been demonstrated in section 3.2.1, nuclear collisions induce a negligible damage production compared with that resulting from electronic excitation in the $(dE/dx)_e$ region above the threshold. A role for elastic-collision-induced damage in the growth phenomenon could then be invoked only in the case where the nature of this damage would be different from that of the electronic-excitation-induced one. It was shown in section 4.2 that this hypothesis is unlikely. Moreover, the amorphous structure cannot accommodate a large variety of defects; positron annihilation experiments have shown that defects of larger than one atomic volume are not stable even at low temperature [40]. Consequently, the influence of elastic collisions on the growth phenomenon observed in the present experiments can hardly be considered. The difference between our interpretation and that of Klaumünzer and co-workers [12, 13, 24, 39] regarding the role of elastic energy loss could then be accounted for by the fact that the irradiations made in Berlin concern much less energetic ions, for which the ratio between the nuclear and the electronic stopping cross sections are much higher.

An amorphous alloy contains a fraction of free volume depending on the preparation technique (melt spinning, sputtering, ion implantation,...) and conditions (cooling rate,...) and on the treatments performed after their elaboration (cold rolling, annealing,...). The concept of free volume is in fact well defined when the alloy temperature is higher than the glass transition temperature T_g. However, in an amorphous alloy prepared by quenching, the difference existing between free volume and vacancy-type defects is weak. As a matter of fact, in Co–Sn amorphous alloys [41] and in amorphous Si [42], the annealing behaviour of the as-prepared and irradiated samples is similar. The discrimination between the defects present before irradiation and those induced by the ion beam is then difficult. Moreover, in

† The product $\eta_0 s_g$ is involved in n_g since equation (12) can be rewritten as

$$n_g = 2\eta_0 s_g c_d(\phi_\infty) N^{2/3}.$$

the growth regime, since the concentration of defects is certainly saturated inside the core of the ion track, it is reasonable to assume that the alloy has lost the 'memory' of the pre-existing free volume. This fact is apparently in conflict with the experimental data reported by Klaumünzer and co-workers [39] which show a direct correlation between the initial fraction of free volume and the value measured for the growth rate. This contradiction could be resolved if we assumed that the initial concentration of free volume is a good indication of the ability to accommodate the presence of disorder in an amorphous alloy.

4.4. Internal stress

The interpretation of the results presented in section 3.2.4 is based on the assumption that the growth phenomenon arises from an 'atomic mobility spike' in which: (i) the atomic mobility is induced by the passage of an ion inside a cylinder of cross section s_g; and (ii) an internal stress polarizes the atomic movements in this cylinder. In this description, the internal stress must present a cylindrical symmetry around the ion path. As an external stress is applied to the sample, the atomic movements are then governed by the total stress (internal and external), so that the symmetry is no longer a cylindrical one. The data presented in figure 11 show that the initial slope D deduced from the resistance curves is stress independent. Since the incubation fluence is also stress independent, the variation of G with the applied stress (figure 12) is only due to a variation of η, i.e. to a variation of the atomic fraction which contributes to the anisotropic change of the sample dimensions.

Assuming that the elementary process involved in the growth consists, as suggested by Ming-Dong Hou *et al* [24], of a reorientation of pairs of atoms perpendicularly to the ion beam and that the direction of these reorientations is driven by the local stress, a rough estimate of the role of an external stress can be attempted. The assumption, as a first approximation, that $\eta_\perp(\theta,\sigma)$ and $\eta_\parallel(\theta,\sigma)$ in equation (10) vary linearly with the external uniaxial stress σ allows us to write

$$\eta_\perp(\theta,\sigma) = \eta_\perp(\theta,0)(1 + A_\perp \sigma \cos\theta) \tag{13a}$$

$$\eta_\parallel(\theta,\sigma) = \eta_\parallel(\theta,0)(1 + A_\parallel \sigma \sin\theta) \tag{13b}$$

where $A_\perp$ and $A_\parallel$ are factors independent of σ but which may depend on the target temperature. Equation (10) then becomes

$$\eta(\theta,\sigma) = \eta(\theta,0) + 2\eta_\perp(\theta,0)(A_\perp \cos^3\theta - 2A_\parallel \sin^3\theta)\sigma. \tag{14}$$

The experimental results presented in figure 12 can be reproduced with a unique set of values: $A_\perp = (8 \pm 2) \times 10^{-3}$ MPa^{-1}; $A_\parallel = -0.1A_\perp$.

The same type of analysis performed in the case of samples irradiated at a temperature of 223 K leads to identical values for $A_\perp$ and $A_\parallel$. This indicates that, in this temperature range, the bias induced by the external applied stress is not thermally activated. Such a model can provide an order of magnitude for the average internal stress $\bar{\sigma}_i$. Indeed, for $\theta = 0$, equation (14) reduces to

$$\eta(0,\sigma) = 2\eta_\perp(0,0)(1 + A_\perp \sigma) \tag{15}$$

which can be rewritten as

$$\eta(0,\sigma) = 2\eta_\perp(0,0)A_\perp(\sigma + \bar{\sigma}_i). \tag{16}$$

According to equation (16), it can be deduced from the data presented in figure 12 that $\bar{\sigma}_i$ is $\sim$ 100 MPa. As a conclusion, the effect of an external stress must be interpreted as a stress-polarized growth rather than a radiation-assisted creep.

4.5. Microscopic approach

An essential problem regarding the mechanisms involved in swift-heavy-ion-irradiation experiments is to understand how energy can be transferred from excited electrons to the target atoms in a way efficient enough to induce atomic displacements leading to both local order modification and growth. Two models have been established in order to account for track formation by electronic excitation in insulators respectively based on the thermal spike [2] and the Coulomb explosion [3] concepts. However, it was often claimed that such models are not valid in the case of metallic systems due to the high density of free electrons which are able to (i) easily spread out the deposited energy, and (ii) screen in a very short time the charge of the atoms highly ionized in the wake of the incident ion. A lot of experimental results (including this work) demonstrate that this statement is no longer valid. It was then interesting to try to extend the above models to the case of metallic systems. Very recently, thermal spike descriptions have been attempted to account for the data obtained on semiconductors [44] as well as on metallic systems [44, 45]. In the following, we present a tentative interpretation of the growth behaviour of amorphous alloys irradiated with swift heavy ions on the basis of a revisited formulation of the Coulomb explosion spike model.

The high electronic energy deposition due to an incoming swift heavy ion induces a high electrostatically unstable continuous cylinder of positively charged ions. In a metallic system, the lifetime τ of this space charge is controlled by the screening of the conduction electrons. The characteristic response time of the electron gas is $\sim \omega_p^{-1}$, where ω_p is the plasma frequency ($\omega_p^{-1} \sim 10^{-16}$ s). This time is much shorter than the characteristic response time of the lattice atoms which is $\sim \omega_D^{-1}$, where ω_D is the Debye frequency ($\omega_D^{-1} \sim 10^{-13}$ s). Nevertheless, in spite of the very short duration of the electron gas perturbation, the highly ionized target atoms may receive an impulse and gain a kinetic energy which can be roughly estimated to be ~ 0.1 eV [13, 46, 47]. One can then assume that the lattice atoms begin to recoil as the space charge is completely screened and consequently as the interatomic potential (and the elastic constants) has recovered its equilibrium value. In the case of sufficiently high electronic stopping power, the space charge cylinder is continuous, so that the radial impulses received by the atoms lying in the ion wake are coherent. Thus, contrary to the Fleisher [3] and Klaumünzer [13, 24, 47] models, where a two-body repulsion is assumed, this coherent motion of atoms leads us to consider that the medium is continuous, which accounts for the response of the material to such a transient excitation. For the sake of simplicity, the theory of linear elasticity in an isotropic medium has been used. Thus, the elastic wave propagation equation in cylindrical geometry can be written as

$$(\partial/\partial r)\{(1/r)(\partial/\partial r)[ru(r,t)]\} = (1/s^2)\partial^2 u(r,t)/\partial t^2 \tag{17}$$

where s is the longitudinal sound velocity, and where $u(r,t)$ quantifies the radial displacement of atoms at a distance r from the ion path and at a time t after the passage of the ion. The initial conditions for this problem of mechanics are

$$u(r,0) = 0 \tag{18a}$$

and

$$(\partial u/\partial t)(r,0) = \dot{u}_0(r) \tag{18b}$$

where $\dot{u}_0(r)$ is the velocity gained by the moving atoms during the lifetime of the space charge. It must be pointed out that a similar problem was treated in the same way (but with different initial conditions) for the case of laser irradiations [48]. Integration of equation (17) with the initial conditions given by equations (18) leads to

$$u(r,t) = \int_0^\infty J_1(\lambda r)\sin(\lambda s t)\,\mathrm{d}\lambda \int_0^\infty \frac{\dot{u}_0(r')}{s} J_1(\lambda r') r'\,\mathrm{d}r'. \tag{19}$$

The induced local dilatation $\delta(r,t)$, which is proportional to the local pressure, can be calculated from equation (19):

$$\delta(r,t) = \frac{\partial u}{\partial r} + \frac{u}{r} = \int_0^\infty \lambda J_0(\lambda r)\sin(\lambda s t)\,\mathrm{d}\lambda \int_0^\infty \frac{\dot{u}_0(r')}{s} J_1(\lambda r') r'\,\mathrm{d}r'. \tag{20}$$

In equation (19) and (20), J_0 and J_1 are Bessel functions of the first kind.

A complete solution for equation (20) can be derived for the initial velocity distribution $\dot{u}_0(r)$ given in equation (18*b*). As an example, let us consider the case where the space charge $\rho(r,t')$ induced by the energy deposited in electronic excitation can be accounted for by the following:

$$\rho(r,t') = \rho_0 \qquad \text{for } r \leqslant b \qquad \text{and } t' \leqslant \tau \tag{21a}$$

$$\rho(r,t') = 0 \qquad \text{for } r > b \qquad \text{or } t' > \tau \tag{21b}$$

where ρ_0 and b are constants which vary with $(\mathrm{d}E/\mathrm{d}x)_e$ and/or the velocity of the incident ions, and τ is the lifetime of the space charge depending on the screening by conduction electrons.

The resulting radial electric field $E(r,t')$ is given by the following:

$$E(r,t') = \frac{e\rho_0}{2\epsilon_0} r \qquad \text{for } r \leqslant b \qquad \text{and } t' \leqslant \tau \tag{22a}$$

$$E(r,t') = \frac{e\rho_0}{2\epsilon_0}\frac{b^2}{r} \qquad \text{for } r > b \qquad \text{and } t' \leqslant \tau \tag{22b}$$

$$E(r,t') = 0 \qquad \forall r \qquad \text{and } t' > \tau \tag{22c}$$

while the resulting velocity distribution at $t' = \tau$ can be written as follows:

$$\dot{u}_0(r) = \frac{e\tau\rho_0}{M_2}\frac{\mathcal{N}}{N}\frac{e\rho_0}{2\epsilon_0} r \qquad \text{for } r \leqslant b \tag{23a}$$

$$\dot{u}_0(r) = 0 \qquad \text{for } r > b \tag{23b}$$

where M_2 is the atomic mass of the target atoms, N is the number of atoms per volume unit of the target and $\mathcal{N}$ is Avogadro's number. The time $t' = \tau$ has been chosen as the time origin for t in equation (17) and (18).

Equation (23*a*) can be rewritten as

$$\dot{u}_0(r) = \alpha(r/b)s \tag{24}$$

where α is a dimensionless parameter.

The dilatation $\delta(r,t)$ appearing in equation (20) is proportional to α and can be expressed as a function of (r/b) and (st/b). Taking for α a value of 0.3, to account for a kinetic energy of 0.1 eV gained by the atoms lying within the ionized cylinder, leads to the variation of the dilatation $\delta(r,t)$ with st/r represented in figure 16. This figure shows that a compression wave ($\delta < 0$) propagates around the ion trajectory and is followed by a strong perturbation of duration $2b/s$. This perturbation leads to an expanded state ($\delta > 0$) which then relaxes slowly. This result suggests that the growth process is linked to the compression wave: the driving force for the atomic motion is the pressure induced by the 'shock wave'. On the other hand, the subsequent expanded state ensures favourable conditions to induce free volume so long as δ remains high enough during a sufficiently long time. This description is entirely consistent with the two-hit model presented above. Indeed the compression wave can only induce atomic motion in a region already damaged, i.e. in a zone where a sufficient amount of free volume has been previously induced by the dilatation wave of a preceding ion impact.

5. Conclusion

Electrical resistance measurements of amorphous Fe–B irradiated with swift heavy ions have demonstrated that electronic energy loss induces atomic displacements in an amorphous metallic target at a rate higher by up to three orders of magnitude than the one obtained with elastic collisions. The atomic displacements certainly consist of a modification of the short-range order of the alloy, similar to that induced by a low-energy ion or electron irradiation. Moreover, the experimental data are in full agreement with the dimensional measurements made in Berlin [12, 13, 24, 39] which have illustrated the occurrence of a dramatic anisotropic growth phenomenon. The application of a uniaxial tensile stress during irradiation has led to the observation of a stress-induced polarization of the growth and has allowed us to estimate an order of magnitude for the internal stress responsible for the deformation.

A two-hit phenomenological model has been developed to account for both the damage production and the growth. In this model, an incident ion is assumed to create a disordered region along its path (track). The anisotropic growth then arises from the passage of a subsequent ion in an already disordered region. A change of the orientation of the target with respect to the beam direction in the course of irradiation has demonstrated that the second hit is entirely responsible for the anisotropy of the deformation, whatever the geometry of the previously damaged region. The model has allowed for the determination of physical parameters, such as track radii, with values close to those previously measured for the case of crystalline metals [11, 32] and inorganic insulators [30, 33, 34].

The phenomenological description of the heavy-ion-irradiation-induced processes presented in this paper does not provide any enlightenment on the way by which electronic excitation leads to atomic rearrangements, i.e. on the very preliminary stage ($\sim 10^{-16}$ s) of the ion–target interaction. For that purpose, an analysis of the results on the basis of a revisited Coulomb explosion mechanism has been proposed. Continuous medium mechanics calculations demonstrate the existence of a compression wave followed by a strong perturbation, which accounts for the observed anisotropic growth.

Finally, it is likely that the mechanisms responsible for the conversion of the energy deposited by electronic excitation into atomic motion can induce the large variety of radiation effects usually seen for the case of low-energy ion irradiation, i.e. in an energy range where elastic collisions overwhelm electronic energy loss. Further developments of the work reported in this paper could then consist of the study of e.g. high-energy ion beam mixing and surface sputtering in metallic systems.

References

[1] Thompson D A 1981 *Radiat. Eff.* **56** 105
[2] Seitz F and Koehler J S 1956 *Solid State Phys.* **2** 305
[3] Fleisher R L, Price P B and Walker R M 1965 *J. Appl. Phys.* **36** 3645
[4] Lesueur D 1975 *Radiat. Eff.* **24** 101
[5] Iwase A, Sasaki S, Iwata T and Nihira T 1987 *Phys. Rev. Lett.* **58** 2950; 1988 *J. Nucl. Mater.* **155** 1188
[6] Dunlop A, Lesueur D and Dural J 1989 *Nucl. Instrum. Methods* B **42** 182
[7] Dunlop A, Legrand P, Lesueur D, Lorenzen N, Morillo J, Barbu A and Bouffard S 1991 *Europhys. Lett.* **15** 765
[8] Dunlop A, Lesueur D, Morillo J, Dural J, Spohr R and Vetter J 1989 *C. R. Acad. Sci. Paris* **309** 1277; 1990 *Nucl. Instrum. Methods* B **48** 419
[9] Paumier E, Toulemonde M, Dural J, Rullier-Albenque F, Girard J P and Bogdanski P 1989 *Europhys. Lett.* **10** 555
[10] Audouard A, Balanzat E, Bouffard S, Jousset J C, Chamberod A, Dunlop A, Lesueur D, Fuchs G, Spohr R, Vetter J and Thomé L 1990 *Phys. Rev. Lett.* **67** 875
[11] Barbu A, Dunlop A, Lesueur D and Averback R S 1991 *Europhys. Lett.* **15** 37
[12] Klaumünzer S and Schumacher G 1983 *Phys. Rev. Lett.* **51** 1987
[13] Klaumünzer S, Hou Ming-Dong and Schumacher G 1986 *Phys. Rev. Lett.* **57** 850
[14] Leteurtre J and Quéré Y 1972 *Defects in Crystalline Solids* vol 6, ed S Amelinckx, R Gevers and J Nihoul (Amsterdam: North-Holland) pp 25–47
[15] Audouard A, Balogh J, Dural J and Jousset J C 1982 *Radiat. Eff.* **62** 161; 1982 *J. Non-Cryst. Solids* **50** 71
[16] Audouard A, Dural J, Jousset J C and Lesueur D 1983 *C. R. Acad. Sci. Paris* Série II **297** 647
[17] Audouard A, Benyagoub A, Thomé L and Chaumont J 1985 *J. Phys. F: Met. Phys.* **15** 1237
[18] Audouard A, Balanzat E, Fuchs G, Jousset J C, Lesueur D and Thomé L 1987 *Europhys. Lett.* **3** 327
[19] Audouard A, Balanzat E, Fuchs G, Jousset J C, Lesueur D and Thomé L 1988 *Europhys. Lett.* **5** 241
[20] Audouard A, Balanzat E, Jousset J C, Fuchs G, Lesueur D and Thomé L 1988 *J. Phys. F: Met. Phys.* **18** L101
[21] Audouard A, Balanzat E, Jousset J C, Fuchs G, Lesueur D and Thomé L 1989 *Radiat. Eff. Defects Solids* **110** 109
[22] Audouard A, Balanzat E, Jousset J C, Fuchs G, Lesueur D and Thomé L 1989 *Nucl. Instrum. Methods* B **39** 18
[23] Bouffard S, Dural J, Levesque F and Ramillon J M 1989 *Ann. Phys., Paris* **4** 395
[24] Hou Ming-Dong, Klaumünzer S and Schumacher G 1990 *Phys. Rev.* B **41** 1144
[25] Audouard A, Balanzat E, Jousset J C, Chamberod A, Fuchs G, Lesueur D and Thomé L 1991 *Phil. Mag.* B **63** 727
[26] Audouard A, Balanzat E, Bouffard S, Jousset J C, Chamberod A, Dunlop A, Lesueur D, Fuchs G, Spohr R, Vetter J and Thomé L 1991 *Nucl. Instrum. Methods* B **59/60** 414
[27] Izui K and Furuno S 1986 *Proc. XIth Int. Conf. Electron Microscopy (Kyoto, 1986)* ed T Imura, S Maruse and T Suzuki (Tokyo: Japanese Society of Electron Microscopy) p 1299
[28] Marfaing J, Marine W, Vidal B, Toulemonde M, Hage Ali M and Stoquert J P 1990 *Appl. Phys. Lett.* **57** 1739
[29] Albrecht D, Armbruster P, Spohr R, Roth M, Shaupert K and Stuhrmann H 1985 *Appl. Phys.* A **37** 37

[30] Fuchs G, Studer F, Balanzat E, Groult D, Toulemonde M and Jousset J C 1987 *Europhys. Lett.* **3** 321
[31] Toulemonde M, Enault N, Fan Jin Yun and Studer F 1990 *J. Appl. Phys.* **68** 1545
[32] Barbu A, Dunlop A, Lesueur D, Averback R S, Spohr R and Vetter J 1991 *Nucl. Tracks Radiat. Meas.* **19** 35
[33] Toulemonde M and Studer F 1988 *Phil. Mag.* A **58** 799
[34] Houpert C, Studer F, Groult D and Toulemonde M 1989 *Nucl. Instrum. Methods* B **39** 720
[35] Balanzat E, Stanley J T, Mairy C and Hillairet J 1985 *Acta Metall.* **33** 785
[36] Gordelik P and Sommer F 1985 *Rapidly Quenched Metals* ed S Steeb and H Warlimont (Amsterdam: Elsevier) p 623
[37] Harmelin M, Etchessahar E, Debuigne J and Bigot J 1988 *Thermochim. Acta* **130** 177
[38] Itoh N and Tanimura K 1990 *J. Phys. Chem. Solids* **51** 717
[39] Hou Ming-Dong, Klaumünzer S and Schumacher G 1987 *Nucl. Instrum. Methods* B **19/20** 16
[40] Audouard A, Moser P, Hautojarvi P and Kauppila J Yli 1983 *Radiat. Eff.* **70** 285
[41] Audouard A, Geny J F, Marchal G and Gerl M 1986 *Phil. Mag.* B **53** 1
[42] Roorda S, Custer J S, Sinke W C, Poate J M, Jacobson D C, Polman A and Spaepen F 1991 *Nucl. Instrum. Methods* B **59/60** 344
[43] Dufour C, Leselier de Chezelles B, Delignon V, Toulemonde M and Paumier E 1992 *Proc. E-MRS Conf. (Strasbourg) 1991* ed P Mazzoldi (Amsterdam: North-Holland) p 61
[44] Paumier E, Toulemonde M and Dufour C 1992 *Phys. Rev.* B **46** 14 362
[45] Szenes G 1992 *Proc. Int. Conf. Physics of Irradiation Effects in Metals (Siofok, Hungary) 1992* (Materials Science Forum) vol 97–99 p 647
[46] Ritchie R H and Claussen C 1982 *Nucl. Instrum. Methods* B **198** 133
[47] Klaumünzer S, Li Chang Lin, Loffler S, Rammensee M, Schumacher G and Neitzert H C 1989 *Radiat. Eff. Defects Solids* **108** 131
[48] Bullough R and Gilman J J 1966 *J. Appl. Phys.* **37** 2283